

# **Knockout of the gene encoding the extracellular matrix protein Sned1 results in craniofacial malformations and early neonatal lethality**

Alexandra Naba<sup>1,\*</sup>, Kyleen Jan<sup>1</sup>, Anna Barqué<sup>1</sup>, Christina L. Nicholas<sup>2,3</sup>, Richard O. Hynes<sup>4,5\*</sup>

<sup>1</sup>: Department of Physiology and Biophysics, College of Medicine, University of Illinois at Chicago, Chicago, Illinois, United States of America

<sup>2</sup>: Department of Orthodontics, College of Dentistry, University of Illinois at Chicago, Chicago, Illinois, United States of America

<sup>3</sup>: Department of Anthropology, College of Liberal Arts and Sciences, University of Illinois at Chicago, Chicago, Illinois, United States of America

<sup>4</sup>: Koch Institute for Integrative Cancer Research, Massachusetts Institute of Technology, Cambridge, Massachusetts, United States of America

<sup>5</sup>: Howard Hughes Medical Institute, Massachusetts Institute of Technology, Cambridge, Massachusetts, United States of America

## **\* Correspondence:**

Alexandra Naba

Email: [anaba@uic.edu](mailto:anaba@uic.edu)

Richard O. Hynes

Email: [rohynes@mit.edu](mailto:rohynes@mit.edu)

## Abstract

---

The extracellular matrix (ECM) is a fundamental component of multicellular organisms that orchestrates developmental processes and controls cell and tissue organization. Mutations in ECM genes or changes in ECM composition, architecture or abundance have been shown to cause or accompany a plethora of diseases including fibrosis, renal, skeletal and vascular diseases and cancers. We previously identified the ECM protein SNED1 in a proteomic screen comparing the ECM of highly and poorly metastatic human mammary tumor xenografts. We further showed that SNED1 promoted breast cancer metastasis and that its level of expression correlated with survival of breast cancer patients. Here we sought to identify the roles of *Sned1* during murine development and physiology. Employing a gene-trap strategy or the introduction of a frameshift mutation, we generated two novel *Sned1* knockout mouse strains. Using these models, we showed that *Sned1* is essential since homozygous ablation of the gene led to early neonatal lethality. *Sned1* is widely expressed in embryos, notably in somitic sclerotomes and neural-crest derivatives. Phenotypic analysis of the few surviving knockout mice obtained revealed a role for *Sned1* in the development of the skeleton and neural-crest-derived craniofacial structures since *Sned1* knockout resulted in growth defects, nasal cavity occlusion, and craniofacial malformations. Altogether our results demonstrate the requisite role for *Sned1* during development and neonatal survival.

## Introduction

---

The extracellular matrix (ECM) is a fundamental component of multicellular organisms. It is a complex and dynamic assembly of hundreds of proteins that provides support to cells and instructs their behaviors (1–3). Knockout mouse models have allowed identification of the instrumental roles of ECM proteins and ECM-protein receptors at multiple steps of embryonic development (4–7).

*SNED1* (Sushi, Nidogen and EGF-like Domains 1), initially named *SNEP* (Stromal Nidogen Extracellular matrix Protein), encodes a secreted protein composed of characteristic domains commonly found in ECM proteins (8,9) including an amino-terminal NIDO domain, 15 EGF-like and calcium-binding EGF-like domains, one or two Follistatin-N-terminal-like (FOLN) domains, (depending on the prediction algorithms (10,11)), a Complement Control Protein (CCP, also known as Sushi domain), and three Type III fibronectin (FN3) domains in the carboxy-terminal region of the protein (Fig 1A). Interrogation of gene and protein databases revealed that orthologues of *SNED1* are found in all sequenced vertebrates, including fish, reptiles, amphibians, birds, and mammals (Fig 1A), but not in lower organisms. Of note, the evolution of vertebrates and mammals was accompanied by the expansion of families of ECM proteins existing in lower organisms (such as the collagens) and the appearance of novel ECM proteins (12–14), such as SNED1. The increasing complexity of the ECM was concomitant with the appearance of novel structures including the neural crest in vertebrates and of mammary glands in mammals (15,16) (see Conclusion).

The murine gene *Sned1* was cloned by Leimeister and collaborators in 2004 from renal stromal cells (17). In this original publication, the authors used *in-situ* hybridization to characterize the sites of expression of *Sned1* at different time points during embryonic development. Their results showed that *Sned1* is broadly expressed, mainly in ectoderm, neural-crest, and mesoderm derivatives including kidneys, adrenal glands, lungs, skeleton, limbs, and the head region (17). However, until recently, no function for Sned1 had been reported.

In a proteomic screen comparing the ECM composition of poorly and highly metastatic human mammary tumors, we identified SNED1 as being more abundant in more aggressive mammary tumors (18). We further showed that it was produced by mammary tumor cells and not by the stromal cells of the tumor microenvironment, and identified the first function of this protein as a metastatic promoter, since knocking down *SNED1*'s expression in tumor cells prevented metastasis (18). We further demonstrated that *SNED1* expression level was predictive of survival of hormone-receptor negative breast cancer patients (18). *Sned1* was found to be up-regulated in murine pancreatic ductal adenocarcinoma (PDAC) cells cultured in a 3-dimensional ECM and which are more resistant to chemotherapeutic drugs, as

compared to cells grown on a 2-dimensional substrate (19). *Sned1* knockdown was also shown to inhibit mutant-p53-driven murine PDAC cell invasion *in vitro* (20).

However, up to now, no functions have been identified for *SNED1* in embryonic development or physiology. To address this, we aimed to knock-out *Sned1* in mice. *Sned1* was targeted using the "knockout-first allele" construct designed through an effort supported by the Wellcome Trust Sanger Institute and the Knockout Mouse Project (21). *Sned1* knockout was achieved using two approaches, a gene-trap strategy and a frameshift mutation strategy (Fig 1B). We also generated a conditional knockout mouse which will be useful in the future to determine the function of *Sned1* in a cell- or time-specific manner. Using these novel mouse models, we demonstrate that *Sned1* is an essential gene, since *Sned1* knockout causes early neonatal (p0 – p2) lethality. Over the course of our studies, we obtained a few homozygous knockout mice which were distinguishable from wild-type and heterozygous littermates by their smaller size and craniofacial malformations, demonstrating that *Sned1* plays significant roles during embryonic development. We propose that altered craniofacial structures might be a potential explanatory factor in the early neonatal lethality of *Sned1* knockout mice.

## Materials and methods

---

### Generation of *Sned1* knockout mice

All experiments involving mice were conducted in conformity with animal protocols approved by MIT's Department of Comparative Medicine and Committee on Animal Care, and by the Committee on Animal Care of the University of Illinois at Chicago in compliance with IACUC guidelines.

Two targeted *Sned1*<sup>tm1a(KOMP)Wtsi</sup> ES cell clones (EPD0300\_5\_02 E02 and F01) from the C57BL/6 JM8.N4 parental ES cell line generated by the Wellcome Trust Sanger Institute (21) were obtained from the KOMP Repository ([www.komp.org](http://www.komp.org)) at UC Davis and cultured on feeder cells using the recommended media including the 2i additives MEK inhibitor PD0325901 and GSK3 inhibitor CHIR99021 (StemGent). Three subclones of each clone were sent to Cell Line Genetics (Madison, WI) for cytogenetic analysis and two subclones of the targeted clone E02 were found to have an apparently normal mouse male karyotype. Cells from subclone E02-2D2 were microinjected into BALB/c blastocysts obtained from natural matings as previously described (22). 10 recipient females each received 14 embryos. 7 pregnant females gave birth to 41 pups, of which 6 showed at least 70% dark coat color against white, BALB/c fur, and allowed establishment of the *Sned1*<sup>tm1a(KOMP)Wtsi</sup> (referred to as *Sned1*<sup>LacZ-Neo</sup>) mouse line. B6.Cg-Tg(ACTFLPe)9205Dym/J (Actin-Flp; Jackson Laboratory stock No. 005703) mice allowing the ubiquitous expression of the Flp recombinase were obtained from MIT's transgenic core facility and were used to generate the *Sned1* floxed *Sned1*<sup>tm1c(KOMP)Wtsi</sup> allele, referred to

as the *Sned1<sup>f</sup>* allele. B6.C-Tg(CMV-cre)1Cgn/J (CMV-Cre) mice allowing the ubiquitous expression of the Cre recombinase were purchased from Jackson Laboratory, stock No. 006054 and were used to generate the null *Sned1tm1d(KOMP)Wtsi* allele, referred to as the *Sned1<sup>-</sup>* allele. Figure 1B shows a schematic view of the alleles. The three mouse strains generated for this study have been deposited to Jackson laboratory: *Sned1<sup>LacZ-Neo</sup>* stock No. 032246, *Sned1<sup>f</sup>* stock No. 032247, and *Sned1<sup>-</sup>* stock No. 032248 and will be made available upon publication of this manuscript.

## Genotyping

DNA was extracted from tail samples from 14-day old pups, or from yolk sacs or tail samples from E18.5 embryos, according to standard procedures and genotyping was performed with the following primers:

*Sned1* (WT allele: 513 bp; floxed allele: 614 bp): Sned1\_F TTCTTATTACACACCGTATGCCAGCC; Sned1\_ttR CTAGTGGGCACTCATTCAAGCAAACC

*Null allele of Sned1* (732 bp):

Sned1\_F TTCTTATTACACACCGTATGCCAGCC; Sned1\_R TCACATGAGCAACACGTTGTAGG

*Neo cassette* (603bp):

Neo\_F GGGATCTCATGCTGGAGTTCTCG; Sned1\_ttR CTAGTGGGCACTCATTCAAGCAAACC

*LoxP site after exon 2* (374 bp):

LoxP\_F GAGATGGCGAACGCAATTAATG; Sned1\_R TCACATGAGCAACACGTTGTAGGG

*Floxed transgene* (725 bp):

Floxed\_F CACTGATATTGTAAGTAGTTGC; Floxed\_R CTAGTGCAGTAGTAGTGATCAGG

*Cre transgene* (700 bp):

Cre\_F TGCTGTACTGGTTATGCGG; Cre\_R TTGCCCTGTTCACTATCCAG

PCR amplification was performed using the Takara ExTaq polymerase. Cycling conditions were: 98°C for 10 sec.; 35 cycles at: 98°C for 10 sec., 60°C for 30 sec., 72°C for 30 sec.; final extension at 72°C for 3 min. Representative genotyping gels are presented in Fig 1C.

## Isolation of mouse embryonic fibroblasts and quantitative PCR

Mouse embryonic fibroblasts (MEFs) were isolated from E13.5 to E15.5 embryos obtained by timed mating of heterozygous *Sned1<sup>WT/LacZ-Neo</sup>* mice. For quantitative PCR (qPCR), RNA was isolated from the cells using the RNeasy kit (Qiagen, Germantown, MD) and cDNA was synthesized by reverse transcription using the First-Strand cDNA Synthesis Kit (Promega, Madison, WI). qPCR reactions were performed using Bio-Rad SYBR Green Supermix (Bio-Rad, Hercules, CA) according to the

manufacturer's instructions. PCR conditions were 95°C for 10 minutes, followed by 40 cycles of 95°C for 20 seconds, 58°C for 30 seconds, and 72°C for 30 seconds. qPCR data analysis was performed using Bio-Rad CFX Manager Software. The following primers were used: Actin\_F: TGTATGAAGGCTTGCTC; Actin\_R: GTCTCAAGTCAGTGTACAGGC; Sned1\_F: GTAGATGGAAGAGGAAGAGTGAG; Sned1\_R CTGTTCTGGTAGCTGGAG.

### Statistical analysis

Goodness-of-fit analysis was performed using a two-tailed chi-square ( $\chi^2$ ) test (GraphPad). This statistical analysis compares expected (Mendelian distribution) and observed numbers of embryos (E18.5) or pups (p21) to determine whether survival correlates with animal genotypes.

### $\beta$ -galactosidase assay

$\beta$ -galactosidase assay (LacZ staining) was performed on whole heterozygous *Sned1<sup>WT/LacZ-Neo</sup>* embryos (E11.5 and E13.5) according to previously published detailed protocols (23,24). For visualization of whole-mount staining, embryos were cleared by incubation in solutions of increasing glycerol and decreasing potassium hydroxide concentrations following a published protocol (25). LacZ-stained embryos were embedded in paraffin and sectioned, sections were then dewaxed and rehydrated, and hematoxylin and eosin counter-staining was performed following standard procedures.

### Microcomputed tomography image acquisition and analysis

An eXplore CT 120 microcomputed tomography ( $\mu$ CT) system (Northridge Tri-Modality Imaging Inc., Chatsworth, CA) was used for *in-vivo* imaging. Mice were imaged under anesthesia (induced at 3% isoflurane in oxygen, maintained at between 2-2.5% during imaging) in groups of 4 in a custom mouse holder. Scanner settings were as follows: 720 views, 360-degree rotation, 70 kVp, 50 mA, 32 ms integration time with 2x2 detector pixel binning (isotropic nominal resolution of 50 microns).

Data were reconstructed using the Parallax Innovations (Ilderton, ON Canada) GPU accelerated reconstruction engine for the eXplore CT120. Reconstructed  $\mu$ CT scans of the mouse crania were converted to TIFF files and imported into 3D Slicer or ImageJ for further analysis.

### Measurement of cranial suture length

Variations in the cranial sutures were visually observed in 3D Slicer (26,27). The nasal, frontal, and sagittal sutures were observed through the transverse plane and were measured antero-posteriorly (in mm), while the coronal sutures were observed through the sagittal plane.

### ***Landmarking and geometric morphometrics***

We selected a total of 30 landmarks (22 traditional coordinate landmarks, 8 sliding semi-landmarks) which were deemed to represent well overall cranial morphology (Supplementary Fig 4). The 8 sliding semi-landmarks were positioned along the nasal suture, as visual observation indicated that nasal and mid-facial morphology may be particularly affected in these mice. To undertake complex phenotyping, we used standard geometric morphometric (GM) methodologies for analyzing 3D shapes. First, a generalized Procrustes analysis (GPA) was run on the raw coordinate landmark data. This procedure scales, rotates, and translates landmark data to align them for further analysis. Importantly, this step (through scaling) reduces size to a separate variable so that shape can be studied in isolation (28). Semi-landmarks were slid, minimizing bending energy, as a part of the GPA. Next, to investigate shape variation in the cohort, we ran a principal components analysis (PCA) on the GPA data. This yielded 19 principal components (PCs), the first four of which each represented >5% of the overall variation, and thus were chosen for further study (28). Statistical significance of each of the first four PCs was assessed using a one-way non-parametric Kruskal-Wallis analysis of variance (ANOVA) by genotype (*Sned1*<sup>WT/WT</sup>, *Sned1*<sup>WT/LacZ-Neo</sup>, *Sned1*<sup>LacZ-Neo/LacZ-Neo</sup>) followed by a Tukey honest significant difference (HSD) test.

### ***Assessment of nasal cavity symmetry and occlusion***

Analyses were conducted using ImageJ software, using the “Multi VFF Opener” plug-in to open the  $\mu$ CT scan files. Variations in nasal cavity symmetry and occlusion were visually observed in 3D Slicer (26,27) and scored.

## **Results**

---

### ***Sned1 knockout results in early neonatal lethality***

*Sned1* knockout was achieved using an IRES:LacZ-trapping cassette (21) inserted in the second intron of *Sned1* (Fig 1B). Decreased expression of *Sned1* was confirmed using RT-qPCR on RNA extracted from mouse embryonic fibroblasts generated from *Sned1*<sup>WT/WT</sup>, *Sned1*<sup>WT/LacZ-Neo</sup>, *Sned1*<sup>LacZ-Neo/LacZ-Neo</sup> mice (Supplementary Fig 1).

We attempted to obtain homozygous knockout mice (*Sned1*<sup>LacZ-Neo/LacZ-Neo</sup>) by intercrossing heterozygous (*Sned1*<sup>WT/LacZ-Neo</sup>) mice. We examined 55 litters born from 16 different breeding pairs of heterozygous mice (representing a total of 334 pups, of which 202 were still alive at weaning). We observed that a significant number of pups died within 48 hours after birth, and, when carcasses could be retrieved for genotyping, we found that the majority of dead neonates were knockout animals. We further observed

that at weaning (p21 +/- 1 day), knockout mice were present in sub-Mendelian ratios ( $\chi^2=20.303$ ; two-tailed p<0.0001) (Table 1). However, Mendelian ratios were observed for E18.5 embryos obtained by C-section (6 litters analyzed,  $\chi^2=1$ ; two-tailed p=0.60605), suggesting that lethality of knockout pups occurred either around or shortly after birth (Table 1).

**Table 1. Numbers of expected and observed E18.5 embryos and 21-day-old pups of each genotype obtained by crossing heterozygous *Sned1*<sup>WT/LacZ-Neo</sup> mice.**

<i>Sned1</i> <sup>WT/LacZ-Neo</sup> x <i>Sned1</i> <sup>WT/LacZ-Neo</sup>	<i>Sned1</i> <sup>WT/WT</sup>	<i>Sned1</i> <sup>WT/LacZ- Neo</sup>	<i>Sned1</i> <sup>LacZ-Neo/LacZ- Neo</sup>	$\chi^2$ <i>p-value</i>
<b>Expected</b>	25%	50%	25%	
<b>E18.5</b>	14 (27.5%)	22 (43.1%)	15 (29.4%)	0.607
<b>Alive at weaning (p21)</b>	54 (26.7%)	130 (64.4%)	18 (8.9%)	<0.0001

We then generated a conditional knockout mouse strain by crossing heterozygous *Sned1*<sup>WT/LacZ-Neo</sup> mice with mice expressing the Flp recombinase under the control of the actin promoter. This resulted in the excision of the IRES: LacZ and Neo cassettes, and the generation of a floxed allele (*Sned1*<sup>f</sup>, Fig 1B). We further crossed conditional knockout mice with mice expressing the Cre recombinase under the control of a CMV promoter to obtain a null allele (*Sned1*<sup>-</sup>, Fig 1B). Heterozygous mice (*Sned1*<sup>WT/-</sup>) were further intercrossed to generate homozygous null mice (*Sned1*<sup>-/-</sup>). We evaluated 13 litters born from 7 different breeding pairs of heterozygous mice (representing a total of 88 pups, of which 63 were still alive at weaning). Similarly to what we observed with the gene-trap allele, a significant number of pups died within 48 hours after birth. When carcasses were retrieved for genotyping, we found that the majority of dead neonates were *Sned1*<sup>-/-</sup> mice. We further observed that at weaning (p21 +/- 1 day), null mice (*Sned1*<sup>-/-</sup>) were present in sub-Mendelian ratios ( $\chi^2=12.492$ ; two-tailed p=0.0019), indicating that null pups had died before that (Table 2). 5 litters were harvested by C-section to examine a total of 44 E18.5 embryos. As observed for the *Sned1*<sup>LacZ-Neo</sup> strain, Mendelian ratios were observed ( $\chi^2=0.364$ ; two-tailed p=0.8338), indicating that lethality of null pups occurred around or shortly after birth (Table 2). Altogether, our data demonstrate that *Sned1* knockout, achieved using two approaches, results in early neonatal lethality.

**Table 2. Numbers of expected and observed E18.5 embryos and 21-day-old pups of each genotype obtained by crossing heterozygous *Sned1*<sup>WT/-</sup> mice.**

<i>Sned1</i> <sup>WT/-</sup> x <i>Sned1</i> <sup>WT/-</sup>	<i>Sned1</i> <sup>WT/WT</sup>	<i>Sned1</i> <sup>WT/-</sup>	<i>Sned1</i> <sup>-/-</sup>	$\chi^2$ <i>p-value</i>
<b>Expected</b>	25%	50%	25%	
<b>E18.5</b>	12 (27.3%)	20 (45.5%)	12 (27.3%)	0.8338
<b>Alive at weaning (p21)</b>	14 (22.2%)	44 (69.8%)	5* (7.9%)	<b>0.0019</b>

\* 1 died at p22; 1 died at p24

Over the course of our study, a few knockout mice survived and we sought to characterize their phenotype to gain insight into the physiological roles of SNED1. Crossing of *Sned* *LacZ-Neo/LacZ-Neo* survivors revealed that surviving *Sned1* knockout mice were fertile although they produced less numerous and smaller litters. Pups obtained by breeding displayed exacerbated phenotypes (in particular, shorter snouts, under-developed mandibles) and only very few of their progeny survived after weaning. Remarkably, the knockout survivors (either *Sned* *LacZ-Neo/LacZ-Neo* or *Sned1*<sup>-/-</sup>) were distinguishable from wild-type and heterozygous littermates by their smaller size and the shape of their head and snout.

### ***Sned1* knockout results in growth defects**

Knockout survivors (either *Sned* *LacZ-Neo/LacZ-Neo* or *Sned1*<sup>-/-</sup>) were smaller than wild-type and heterozygous littermates (Fig 2A). At p14, knockout pups weighed significantly less than wild-type and heterozygous littermates (Fig 2B and Supplementary Fig 2A). This reduced body weight was readily detectable in p0.5 neonates (Fig 2C). Interestingly, we also observed that no milk was present in the stomachs of p0.5 knockout neonates whereas milk was present in wild-type and heterozygous littermates (Fig 2D). Together with the observation that some neonates presented under-developed mandibles (Fig 2E), we can hypothesize that the observed reduced body weight and neonatal lethality could be attributed, in part, to a decreased ability of knockout pups to suckle or ingest milk.

### ***Sned1* is expressed in skeletal and craniofacial precursors.**

We took advantage of the LacZ reporter gene expressed under the control of the *Sned1* promoter to determine in which tissues *Sned1* was expressed during development. Whole-mount LacZ staining

revealed that the *Sned1* promoter is broadly active at the two time-points examined, embryonic days 11.5 (Fig 3A) and 13.5 (Fig 3C). At E11.5, LacZ staining was observed in mesodermal derivatives including the ventro-medial cells of the somites (Figs 3A and 3C) which will undergo epithelial-to-mesenchymal transition (EMT) to form the sclerotomes which will, in turn, give rise the vertebrae and the ribs. LacZ staining was also detected in the pharyngeal arches (29) (Fig 3B), structures originating from the cephalic neural crest cells (NCC), which also undergo EMT when they detach from the neural tube, and will give rise to precursors of the nose, mandible (Meckel's cartilage) and tongue (visible at E13.5, Fig 3E). In addition, staining was detected in the lung buds (Fig 3C, right panel), as previously reported (17) and in Rathke's pouch, a structure deriving from the oral ectoderm which will give rise to the adenohypophysis of the pituitary gland. At E13.5, staining was visible in the cartilage primordium of the ribs and the vertebrae (Figs 3D, and 3G). Of note, the Lac-Z staining intensity followed the antero-posterior axis, with the posterior somites being the last to differentiate and the most intensely stained (Fig 3G, right panel). Staining was also observed in the limb buds (Figs 3F, and 3G), in particular in the interdigital space that will undergo apoptosis to form the digits (Fig 3F), the choroid plexus (Fig 3G, middle and left panel), and in the mesenchyme surrounding the dorsal root ganglia. In addition, staining was observed in the head region, in the derivatives of the pharyngeal arches including the tongue and nose, the vomero-nasal organ, a chemoreceptive organ part of the olfactory system. Our results confirm and extend the previously published study reporting the expression of *Sned1* using *in-situ* hybridization (17), and with gene expression data reporting *Sned1* expression in the mandible and frontonasal region of E10.5 to E12.5 embryos (30,31).

### ***Sned1* knockout mice present cranial bone malformations**

In addition to their small size, we observed that the knockout survivors were also distinguishable from wild-type and heterozygous littermates by their shorter snouts and abnormal head shape (Fig 4A). Because *Sned1* is expressed in structures that give rise to the craniofacial bones and cartilage, we sought to examine the skulls of wild-type, heterozygous and *Sned1* knockout mice using micro-computed tomography ( $\mu$ CT) (Fig 4A). We measured the length of the different calvarial sutures (Supplementary Fig 3A) including the nasal (anterior tip of nasal bones to premaxillary suture; Fig 4B), frontal (premaxillary suture to coronal suture; Supplementary Fig 3B), and sagittal suture (coronal to interparietal suture; Supplementary Fig 3C). Knockout mice showed statistically significantly shorter nasal sutures as compared to wild-type ( $p=0.0036$ ) or heterozygous ( $p=0.0051$ ) mice (Fig 4B). Neither

frontal nor sagittal sutures showed statistically significant differences between groups, although, in both cases, there was a trend towards shorter sutures in the knockout group (Supplementary Figs 3B and 3C). We further employed geometric morphometric analysis to quantify complex 3D phenotypic variations in craniofacial morphology between mice of different genotypes (Supplementary Fig 4). Principal component analysis identified one component (PC1) which represents 30.05% of the overall variation and describes differences in cranial vault shape and nasal bridge morphology. PC1 showed statistically significant differences across the three groups ( $p=0.027$ , Fig 4C). Animals at the maximum extreme of variation along PC1 (PC1 max, wild-type and heterozygous mice) tended to show relatively flatter (supero-inferiorly) and medio-laterally narrower neurocrania, narrower midfaces (at the zygoma), and convexity of the nasal bridge. Those at the minimum extreme of variation along PC1 (PC1 min, knockout mice), in contrast, showed concavity of the nasal bridge, relatively shorter snouts, wider faces and neurocrania, and more supero-inferiorly expanded neurocrania (Fig 4D).

A Tukey HSD test revealed that the overall statistical significance in PC1 was driven by differences between the wild-type and knockout groups ( $p=0.048$ ) and between the heterozygote and knockout groups ( $p=0.017$ ) while the comparison of the heterozygous and wild-type mice was not statistically significantly different ( $p=0.99$ ) (Fig 4E). Although the mechanism by which *Sned1* controls nasal bridge formation remains unknown, we can hypothesize that it results from a weakening of the nasal septum, the cartilaginous structure that supports the ossified nasal bridge.

### ***Sned1* knockout mice present asymmetrical and occluded nasal cavities**

The observation that *Sned1* is expressed in structures giving rise to the nose (Fig 3B) and that *Sned1* knockout mice present nasal bridge collapse (Fig 4A, arrow) prompted us to further evaluate the anatomy of the nasal cavity of the animals. We observed that the three knockout neonates ( $p0.5$ ) presented at least partial nasal occlusion, defined as a contact between the soft tissues forming the wall of the airways, whereas none of the wild-type animals presented occlusion (Fig 4F, Supplementary Files 1, 2, and 3). In the cohort of adult mice, 2 out of the 5 knockout mice presented markedly asymmetrical nasal cavities, whereas 9 out of 10 heterozygous and all 4 wild-type mice had symmetrical cavities (Fig 4G, Supplementary Files 4, 5, and 6). In addition, 2 out of the 5 knockout mice presented partial occlusion, in contrast to all wild-type and heterozygous mice which presented no occlusion. Together with nasal obstruction, these observations support the hypothesis that the *Sned1* knockout neonates may not survive because of impaired nasal respiration.

## Discussion and conclusions

---

Here we report the generation of *Sned1* knockout mice and their phenotypic analysis. We showed that *Sned1* is essential during development, since most knockout mice die prematurely within 2 days of birth and the few surviving animals exhibit severe growth defect and craniofacial malformations. It is worth noting that the adult mice on which the phenotypic analyses were conducted are likely to present less severe phenotypes because they survived. Follow-up studies are now required to understand which compensatory mechanisms intervened and led to certain animals surviving whereas the majority of *Sned1* knockout neonates did not survive past post-natal day 2. Of note, despite the broad pattern of expression of *Sned1* in murine embryos, the only phenotypes discerned in this study relate to overall growth and craniofacial features. The surviving *Sned1* knockout adults did not present other overt anomalies. In addition, morphological and histological analysis of two litters of p.0.25 neonates (including two knockout animals) and of some of the knockout pups that were found dead did not reveal gross anomalies in tissues apart from the head and tail regions (data not shown).

Further investigations are also required to decipher the precise cellular and molecular mechanisms controlled by *Sned1* and underlying growth defect and craniofacial morphogenesis. We previously discovered SNED1 as an ECM protein promoting breast cancer metastasis (18). Here, we report the expression of *Sned1* during embryonic development in structures that will undergo epithelial-to-mesenchymal transition (EMT), including the sclerotomes or have undergone EMT, such as the neural-crest derivatives (32). The parallel has been drawn between developmental EMT and carcinoma metastasis, since in both cases, epithelial cells lose cell-cell junctions, up-regulate ECM genes such as fibronectin, remodel their adhesions to the ECM and acquire a migratory phenotype (33,34). It would thus be interesting to determine whether SNED1 regulates this process both in development and in cancer.

Sequence analysis revealed that orthologues of *Sned1* are found in all sequenced vertebrates, but not in lower organisms (Fig 1A). In addition, two consensus potential binding sites (RGD and LDV, Fig 1A) for integrins (35,36), which are known ECM protein receptors, are present in the amino-terminal region of mammalian sequences of *Sned1* (Fig 1A), suggesting that the protein has further evolved, likely to support the development of mammalian-specific structures. One RGD motif is also found in the carboxy-terminal region of the zebrafish sequence. It would thus be important to investigate whether the putative integrin-binding sites do engage these ECM receptors, and if so, if this is how *Sned1* governs skeletal and craniofacial morphogenesis. It is also crucial to study both the signaling pathways regulating *Sned1* and the pathways activated downstream of *Sned1*. Of note, *Sned1* was among the most significantly up-

regulated genes in neural-crest-cell-specific *Tgfb2* knockout mice (*Tgfb2<sup>fl/fl</sup>*; *Wnt1-Cre*) presenting abnormal palate closure (clefting) (37). Although cleft or lip palate were not observed in *Sned1* knockout mice, this observation may suggest that *Sned1* is regulated by the TGFβ signaling pathways. Future mechanistic investigations will benefit from the conditional *Sned1* knockout mouse generated in this study which will be instrumental in determining the functions of *Sned1* in a cell- or tissue-specific and time-specific manner. Further study of the roles of *Sned1* in craniofacial development in mice may also shed light on fundamental processes that, when altered, lead to craniofacial malformations in humans (38).

In humans, *SNED1* is localized on the long arm of chromosome 2 (2q37.3). Deletion of 2q37 in human patients is characterized by mental retardation, facial dysmorphism and skeletal abnormalities including short stature (39–41). *SNED1* had not been cloned when those studies were published. In light of the present study, it would be interesting to determine to what extent the craniofacial phenotype of 2q37 patients can be attributed to the loss of *SNED1*.

## Acknowledgements

---

The authors wish to acknowledge Dr. Aurora Burds Connor and Noranne Enzer from the ES Cell and Transgenics Facility (MIT) for their help generating the *Sned1* mouse lines, Kathleen Cormier from The Hope Babette Tang (1983) Histology Facility (MIT) for her help with preparation and sectioning of histological samples, Milton Cornwall-Brady and Dr. Scott Malstrom from the Animal Imaging & Preclinical Testing Core Facility (MIT) for their assistance with uCT image acquisition, and Lisa Billings and Katherine De La Hoz from the MIT Department of Comparative Medicine for their assistance with mouse husbandry. The authors also wish to acknowledge Dr. Patrick Murphy (Hynes lab) for noticing the craniofacial anomalies of the *Sned1* knockout mice, Ying Huang and Zhigang Jiang (Hynes lab) for assistance with genotyping, Martin Davis (Naba lab) for assistance with genotyping and mouse colony maintenance, and the members of the Hynes and Naba laboratories for helpful discussions. The *Sned1* mouse strains used for this research project were created from ES cell clone EPD0300\_5\_E02, obtained from the KOMP Repository ([www.komp.org](http://www.komp.org)) and generated by the Wellcome Trust Sanger Institute. Targeting vectors used were generated by the Wellcome Trust Sanger Institute and the Children's Hospital Oakland Research Institute as part of the Knockout Mouse Project (3U01HG004080).

## References

---

1. Hynes RO, Naba A. Overview of the Matrisome -An Inventory of Extracellular Matrix Constituents and Functions. *Cold Spring Harb Perspect Biol*. 2012 Jan 1;4(1):a004903–a004903.
2. Rozario T, DeSimone DW. The extracellular matrix in development and morphogenesis: a dynamic view. *Dev Biol*. 2010 May 1;341(1):126–40.
3. Bonnans C, Chou J, Werb Z. Remodelling the extracellular matrix in development and disease. *Nat Rev Mol Cell Biol*. 2014 Nov 21;15(12):786–801.
4. DeSimone DW, Mecham RP, editors. *Extracellular Matrix in Development* [Internet]. Berlin, Heidelberg: Springer Berlin Heidelberg; 2013. (Biology of Extracellular Matrix). Available from: <http://link.springer.com/10.1007/978-3-642-35935-4>
5. Czirok A, Rongish BJ, Little CD. Extracellular Matrix Dynamics in Early Development. In: *Extracellular Matrix in Development* [Internet]. Springer, Berlin, Heidelberg; 2013 [cited 2018 Jul 2]. p. 19–36. (Biology of Extracellular Matrix). Available from: [https://link.springer.com/chapter/10.1007/978-3-642-35935-4\\_2](https://link.springer.com/chapter/10.1007/978-3-642-35935-4_2)
6. George EL, Hynes RO. Gene targeting and generation of mutant mice for studies of cell-extracellular matrix interactions. *Methods Enzymol*. 1994;245:386–420.
7. Extracellular Matrix in Development and Disease, Volume 15 - 1st Edition [Internet]. Available from: <https://www.elsevier.com/books/extracellular-matrix-in-development-and-disease/unknown/978-0-444-51846-0>
8. Hohenester E, Engel J. Domain structure and organisation in extracellular matrix proteins. *Matrix Biol*. 2002 Mar;21(2):115–28.
9. Naba A, Clauser KR, Hoersch S, Liu H, Carr SA, Hynes RO. The matrisome: in silico definition and in vivo characterization by proteomics of normal and tumor extracellular matrices. *Mol Cell Proteomics*. 2012 Apr;11(4):M111.014647.
10. Letunic I, Doerks T, Bork P. SMART: recent updates, new developments and status in 2015. *Nucleic Acids Res*. 2015 Jan 28;43(D1):D257–60.
11. Finn RD, Attwood TK, Babbitt PC, Bateman A, Bork P, Bridge AJ, et al. InterPro in 2017—beyond protein family and domain annotations. *Nucleic Acids Res*. 2017 Jan 4;45(D1):D190–9.
12. Özbek S, Balasubramanian PG, Chiquet-Ehrismann R, Tucker RP, Adams JC. The Evolution of Extracellular Matrix. *Mol Biol Cell*. 2010 Dec 15;21(24):4300–5.

13. Huxley-Jones J, Pinney JW, Archer J, Robertson DL, Boot-Handford RP. Back to basics – how the evolution of the extracellular matrix underpinned vertebrate evolution. *Int J Exp Pathol.* 2009 Apr;90(2):95–100.
14. Hynes RO. The evolution of metazoan extracellular matrix. *J Cell Biol.* 2012 Mar 19;196(6):671–9.
15. Bronner ME, LeDouarin NM. Evolution and Development of the Neural Crest: An Overview. *Dev Biol.* 2012 Jun 1;366(1):2–9.
16. Muñoz WA, Trainor PA. Neural crest cell evolution: how and when did a neural crest cell become a neural crest cell. *Curr Top Dev Biol.* 2015;111:3–26.
17. Leimeister C, Schumacher N, Diez H, Gessler M. Cloning and expression analysis of the mouse stroma marker Snep encoding a novel nidogen domain protein. *Dev Dyn.* 2004 Jun;230(2):371–7.
18. Naba A, Clauser KR, Lamar JM, Carr SA, Hynes RO. Extracellular matrix signatures of human mammary carcinoma identify novel metastasis promoters. *eLife [Internet].* 2014;3:e01308. Available from: <http://elife.elifesciences.org/content/3/e01308>
19. Longati P, Jia X, Eimer J, Wagman A, Witt M-R, Rehnmark S, et al. 3D pancreatic carcinoma spheroids induce a matrix-rich, chemoresistant phenotype offering a better model for drug testing. *BMC Cancer.* 2013 Feb 27;13:95.
20. Weissmueller S, Manchado E, Saborowski M, Morris JP, Wagenblast E, Davis CA, et al. Mutant p53 drives pancreatic cancer metastasis through cell-autonomous PDGF receptor beta signaling. *Cell.* 2014 Apr 10;157(2):382–94.
21. Skarnes WC, Rosen B, West AP, Koutsourakis M, Bushell W, Iyer V, et al. A conditional knockout resource for the genome-wide study of mouse gene function. *Nature.* 2011 Jun 16;474(7351):337–42.
22. Esmail MY, Qi P, Connor AB, Fox JG, García A. Generating Chimeric Mice by Using Embryos from Nonsuperovulated BALB/c Mice Compared with Superovulated BALB/c and Albino C57BL/6 Mice. *J Am Assoc Lab Anim Sci JAALAS.* 2016;55(4):400–5.
23. Burn SF. Detection of β-galactosidase activity: X-gal staining. *Methods Mol Biol Clifton NJ.* 2012;886:241–50.
24. Gierut JJ, Jacks TE, Haigis KM. Whole-Mount X-Gal Staining of Mouse Tissues. *Cold Spring Harb Protoc.* 2014 Apr 1;2014(4):pdb.prot073452.
25. Schatz O, Golenser E, Ben-Arie N. Clearing and photography of whole mount X-gal stained mouse embryos. *BioTechniques.* 2005 Nov;39(5):650, 652, 654 passim.

26. Fedorov A, Beichel R, Kalpathy-Cramer J, Finet J, Fillion-Robin J-C, Pujol S, et al. 3D Slicer as an Image Computing Platform for the Quantitative Imaging Network. *Magn Reson Imaging*. 2012 Nov;30(9):1323–41.
27. Pieper S, Halle M, Kikinis R. 3D SLICER. In: Proceedings of the 1st IEEE International Symposium on Biomedical Imaging: From Nano to Macro 2004 [Internet]. IEEE International Symposium on Biomedical Imaging ISBI 2004; p. 632:635. Available from: <http://www.spl.harvard.edu/publications/item/view/91>
28. Geometric Morphometrics for Biologists - 2nd Edition [Internet]. Available from: <https://www.elsevier.com/books/geometric-morphometrics-for-biologists/zelditch/978-0-12-386903-6>
29. Parada C, Chai Y. Chapter Two - Mandible and Tongue Development. In: Chai Y, editor. Current Topics in Developmental Biology [Internet]. Academic Press; 2015 [cited 2018 Jun 26]. p. 31–58. (Craniofacial Development; vol. 115). Available from: <http://www.sciencedirect.com/science/article/pii/S0070215315000599>
30. Feng W, Leach SM, Tipney H, Phang T, Geraci M, Spritz RA, et al. Spatial and Temporal Analysis of Gene Expression during Growth and Fusion of the Mouse Facial Prominences. *PLOS ONE*. 2009 Dec 16;4(12):e8066.
31. Tipney HJ, Leach SM, Feng W, Spritz R, Williams T, Hunter L. Leveraging existing biological knowledge in the identification of candidate genes for facial dysmorphology. *BMC Bioinformatics*. 2009 Feb 5;10(2):S12.
32. Thiery JP, Acloque H, Huang RYJ, Nieto MA. Epithelial-Mesenchymal Transitions in Development and Disease. *Cell*. 2009 Nov 25;139(5):871–90.
33. Gallik KL, Treffy RW, Nacke LM, Ahsan K, Rocha M, Green-Saxena A, et al. Neural crest and cancer: Divergent travelers on similar paths. *Mech Dev*. 2017 Dec 1;148:89–99.
34. Brabletz T, Kalluri R, Nieto MA, Weinberg RA. EMT in cancer. *Nat Rev Cancer*. 2018 Feb;18(2):128–34.
35. Ruoslahti E. RGD and other recognition sequences for integrins. *Annu Rev Cell Dev Biol*. 1996;12:697–715.
36. Campbell ID, Humphries MJ. Integrin Structure, Activation, and Interactions. *Cold Spring Harb Perspect Biol*. 2011 Mar 1;3(3):a004994–a004994.
37. Pelikan RC, Iwata J, Suzuki A, Chai Y, Hacia JG. Identification of Candidate Downstream Targets of TGF $\beta$  Signaling During Palate Development by Genome-Wide Transcript Profiling. *J Cell Biochem*. 2013 Apr;114(4):796–807.

38. Van Otterloo E, Williams T, Artinger KB. The old and new face of craniofacial research: How animal models inform human craniofacial genetic and clinical data. *Dev Biol.* 2016;15;415(2):171–87.
39. 2q37 deletion syndrome [Internet]. Available from: <https://www.omim.org/entry/600430>
40. Shrimpton AE, Braddock BR, Thomson LL, Stein CK, Hoo JJ. Molecular delineation of deletions on 2q37.3 in three cases with an Albright hereditary osteodystrophy-like phenotype. *Clin Genet.* 2004 Dec;66(6):537–44.
41. Aldred MA, Sanford ROC, Thomas NS, Barrow MA, Wilson LC, Brueton LA, et al. Molecular analysis of 20 patients with 2q37.3 monosomy: definition of minimum deletion intervals for key phenotypes. *J Med Genet.* 2004 Jun;41(6):433–9.

## Figure legends

---

### Figure 1. Sned1 phylogeny, alleles, and genotyping strategy

- A.** Schematic representation of the protein domains of SNED1 and alignment between the human (*Hs*) sequence of SNED1(UniProt accession Q8TER0) and orthologs found in mouse (*M. musculus*, *Mm*; UniProt accession Q70E20); rat (*R. Norvegicus*, *Rn*; UniProt accession Q5ZQU0); chicken (*G. gallus*, *Gg*; UniProt accession A0A1D5P671); zebrafish (*D. rerio*, *Dr*; UniProt accession E7F2S5); and frog (*X. laevis*, *Xl*; UniProt accession A0A1L8GAZ2). Alignment was performed using Protein BLAST (<https://blast.ncbi.nlm.nih.gov/Blast.cgi?PAGE=Proteins>). Percent identity and percent homology are indicated for each domain or fragment of SNED1 and for the full-length proteins. Protein length in amino acid (aa) is also indicated.
- B.** Schematic overview of the different alleles *Sned1*<sup>WT</sup>, *Sned1*<sup>LacZ-Neo</sup> (*KOMP tm1a*), *Sned1*<sup>f</sup> (*KOMP tm1c*), and *Sned1*<sup>-</sup> (*KOMP tm1d*). Arrows indicate primers used for genotyping.
- C.** PCR genotyping of genomic DNA isolated from tail samples of *Sned1*<sup>WT/LacZ-Neo</sup> (left panel), *Sned*<sup>WT/f</sup> (middle panel), and *Sned*<sup>WT/-</sup> (right panel) mice.

### Figure 2. Surviving *Sned1* knockout mice present growth defects

- A.** Representative pictures of heterozygous (left) and knockout (right) 21-day-old mice illustrate the reduced size of surviving knockout mice.
- B.** Bar graph represents the weight of 14-day-old pups. Numbers of mice per gender and genotype are indicated in the bars. Data are presented as means ± S.E.M.
- C.** Bar graph represents weight of 0.5-day-old neonates. Numbers of mice per genotype are indicated in the bars. Data are presented as means ± S.E.M.
- D.** Representative litter of p0.5 neonates. Black arrows indicate the presence of milk the stomach of wild-type and heterozygous mice. Note the absence of milk in the stomach of knockout neonates. Blue arrow points to the tails of knock-out neonates which fail to curl, perhaps related to the strong expression in tail-bud somites and mesoderm (Fig 3G.)
- E.** A p1.5 *Sned1*<sup>-/-</sup> neonate was found dead and lacks entirely a lower jaw (right panels). Picture of an age-matched wild-type littermate is provided for comparison (left panel).

### Figure 3. Patterns of expression of *Sned1* gene during embryogenesis

- A.** Whole-mount β-galactosidase assay (LacZ staining) performed on heterozygous E11.5 *Sned1*<sup>WT/LacZ-Neo</sup> embryo show the wide expression of Sned1 during development.

- B.** Sagittal section of the head region of Lac-Z-stained E11.5 LacZ *Sned1*<sup>WT/LacZ-Neo</sup> embryo. 1, 2, 3, and 4 represent the branchial arches; NP: nasal process; RP: Rathke's pouch.
- C.** Sagittal sections of Lac-Z-stained E11.5 LacZ *Sned1*<sup>WT/LacZ-Neo</sup> embryo (left panel: lateral section; right panel: across the midline). Lu B, lung bud; So, somites; DRG, dorsal root ganglia.
- D.** Whole-mount β-galactosidase assay (LacZ staining) performed on heterozygous E13.5 *Sned1*<sup>WT/LacZ-Neo</sup> embryo show the wide expression of Sned1 during development.
- E.** Transverse section of the head region of LacZ-stained E13.5 LacZ *Sned1*<sup>WT/LacZ-Neo</sup> embryo. MC: site of apposition in the midline of Meckel's cartilages; T, tongue; VO, vomeronasal organ; NS, cartilage primordium of nasal septum.
- F.** Section of paw from LacZ-stained E13.5 LacZ *Sned1*<sup>WT/LacZ-Neo</sup> embryo. Arrows indicate interdigital spaces).
- G.** Sagittal sections of Lac-Z-stained E13.5 LacZ *Sned1*<sup>WT/LacZ-Neo</sup> embryo (from left to right: lateral to the midline). HL, forelimb; HL, hindlimb; DRG, dorsal root ganglia; V, cartilage primordium of the vertebrae; CP, choroid plexus.

**Figure 4. *Sned1* knockout results in craniofacial malformations**

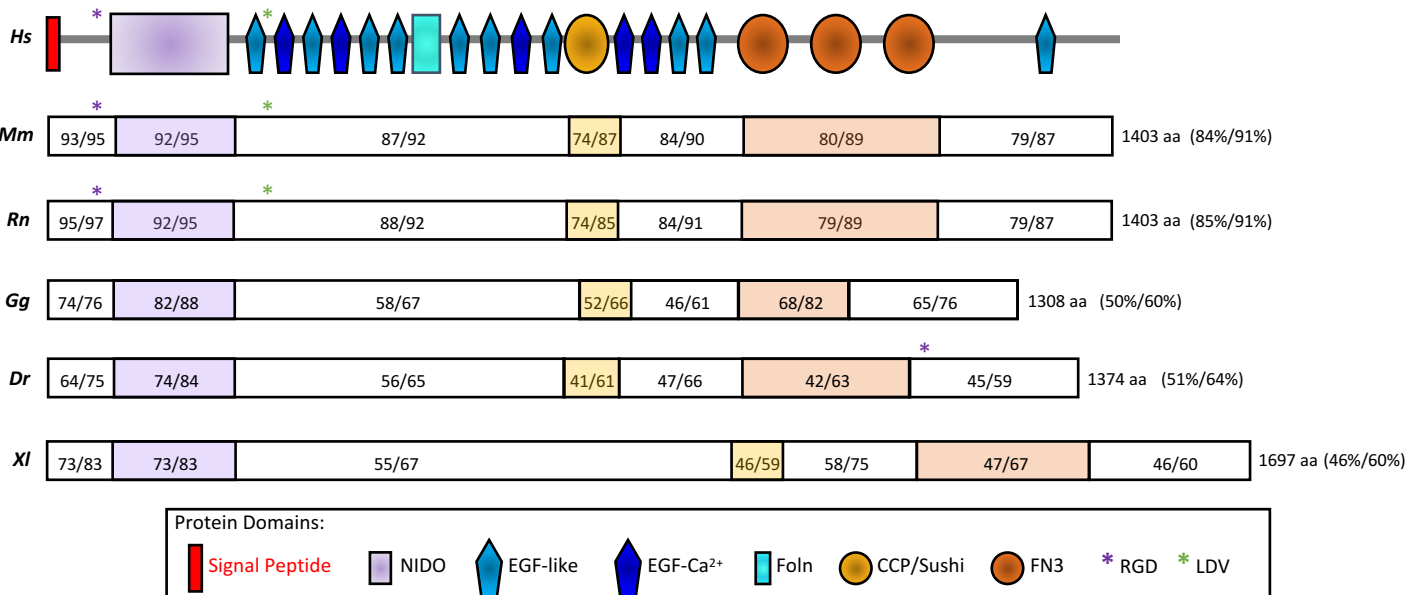
- A.** μCT scans show examples of variation in skull morphology based upon genotype. Note the nasal bridge collapse in the depicted *Sned1*<sup>LacZ-Neo/ LacZ-Neo</sup> mouse (arrows).
- B.** Nasal suture length was measured from the anterior tip of nasal bones to premaxillary suture (Supplementary Fig 3A). Knockout mice (black triangles) showed statistically significantly shorter nasal sutures than wild-type (white circles; p=0.0036) or heterozygous (grey squares; p=0.0051) mice.
- C.** Scatterplot of PC1 and PC2 for variation in the mouse cranial morphology. Knockout mice are clustered towards the negative end of the range (PC1 min), while wild-type and heterozygous mice are clustered towards the positive end of the range (PC1 max).
- D.** Wireframes depicting variation of the cranial shape. Grey dots represent the consensus cranium shape, black dots represent the shape depicted by minimum (PC1 min, upper panel) or the maximum (PC1 max, lower panel) of the range of variation. Left panels are side views of the mouse cranium, right panels are top views. Upper panel: Knockout mice tend to show superior-inferiorly broader neurocrania, shorter snouts (dotted arrow) with a concave nasal bridge, and relatively wider faces at the zygoma. Lower panel: wild-type and heterozygous mice tend to show narrower crania, longer snouts (black arrow), with a convex nasal bridge, and relatively narrower heads. Note the almost complete overlap between the consensus cranium shape (grey dots) and the wild-type and heterozygous mice (black dots) along PC1 max, and the divergence of the knockout mice (black dots) along PC1 min.

**E.** Boxplot of PC1 data by mouse genotype. The knockout mice showed greater variability in craniofacial shape and were statistically significantly different from both the wild-type ( $p=0.048$ ) and heterozygous ( $p=0.017$ ) mice along PC1.

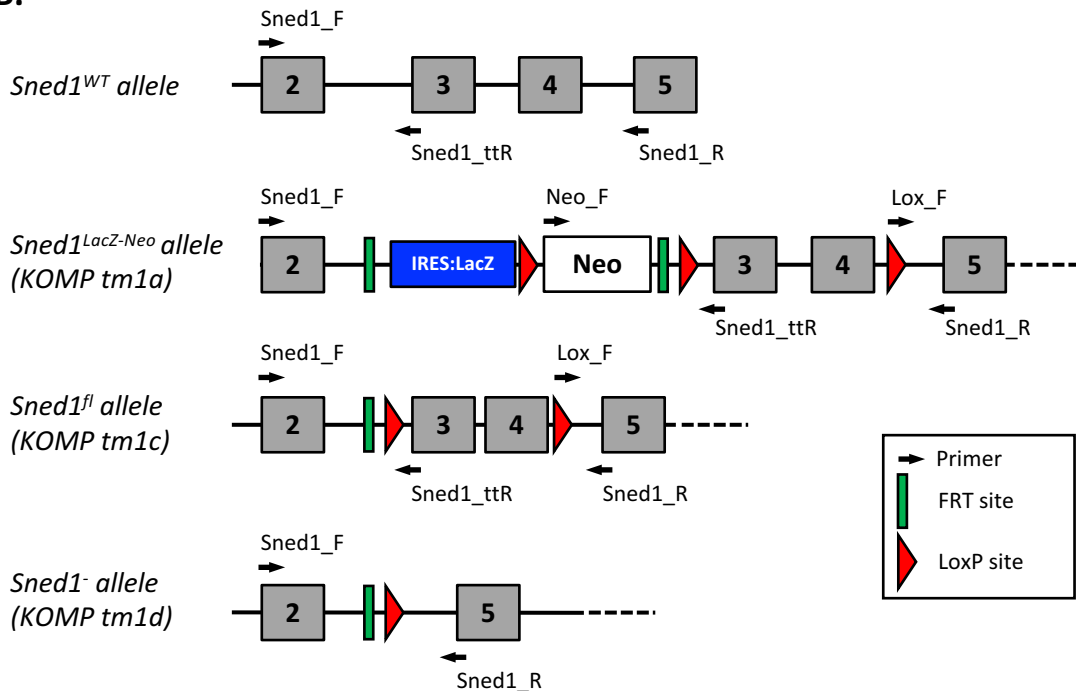
**F - G.** Assessment of the degree of occlusion and asymmetry of the nasal cavity of 22 p0.5 neonates (**F**) and 19 6-month-old adult mice (**G**) was conducted using 3D Slicer. Representative  $\mu$ CT images are shown in the left panels and phenotype quantification on the right panels. Airway passages appear dark and denser tissues such as cartilage and bone tissues appear in white or lighter shades of gray. Arrows indicate occlusions and asymmetries. Representative and complete  $\mu$ CT scan files of mice from each genotype are provided as Supplementary content.

# Figure 1.

**A.**



**B.**



**C.**

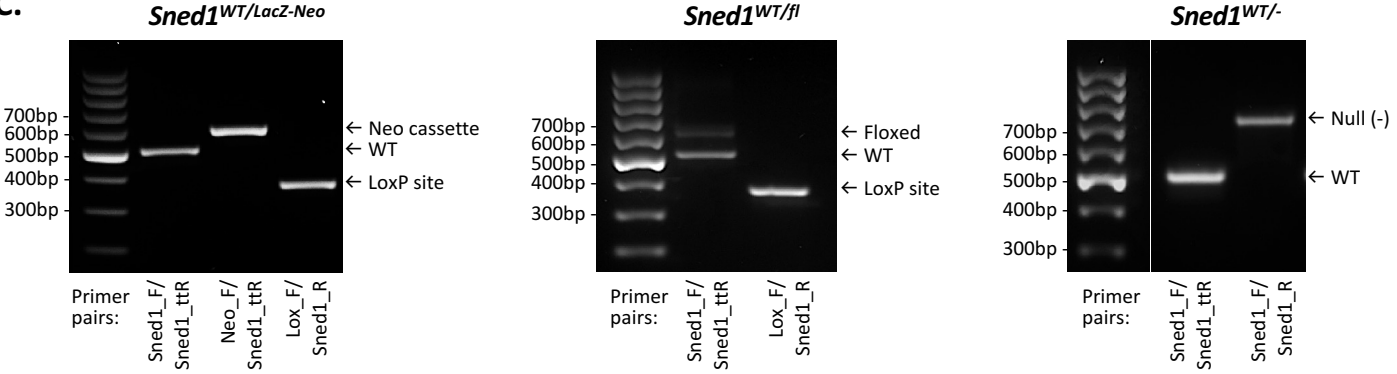
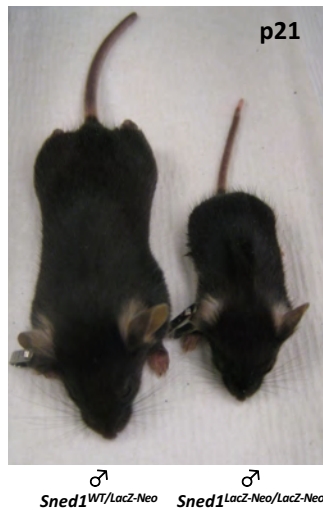
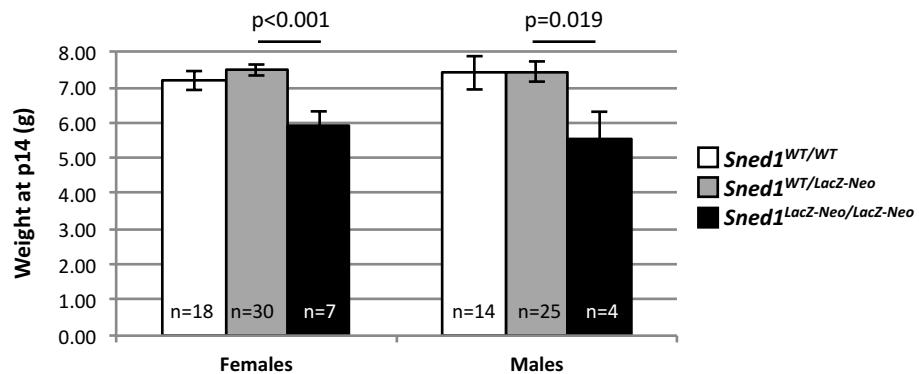


## Figure 2.

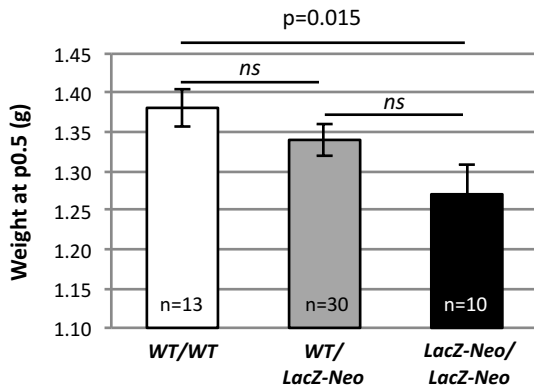
A.



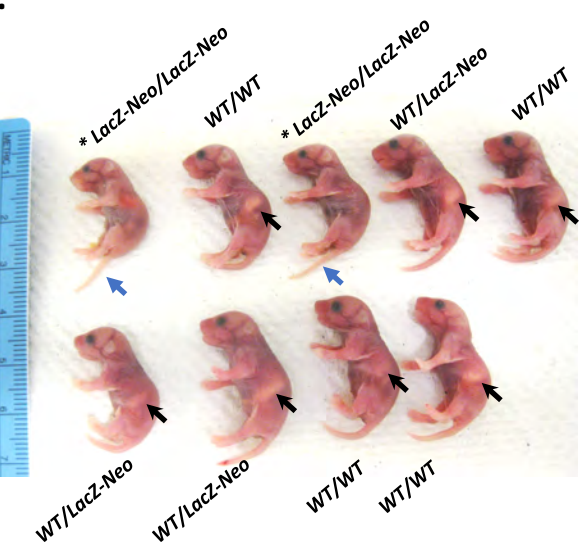
B.



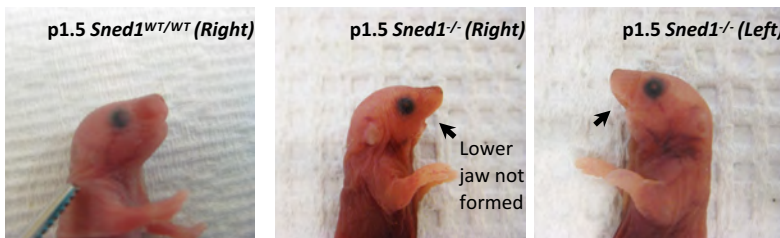
C.



D.

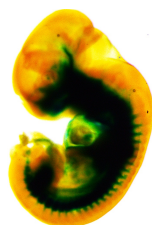
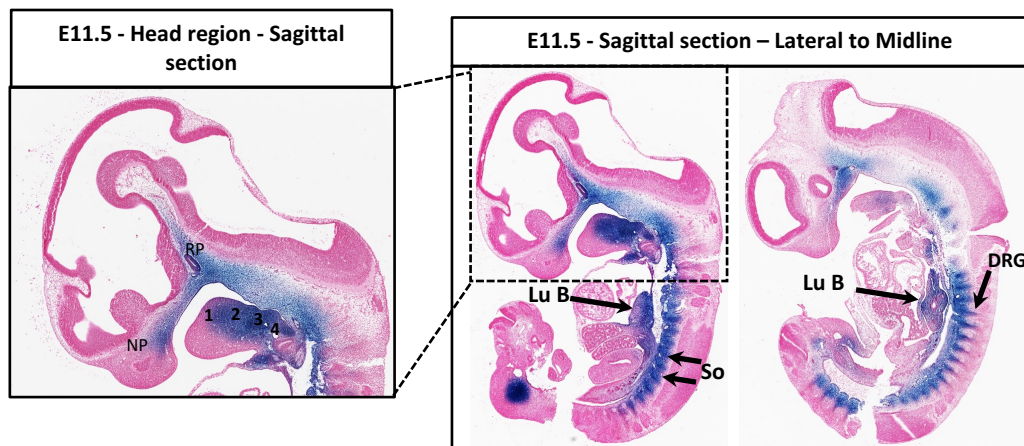


E.

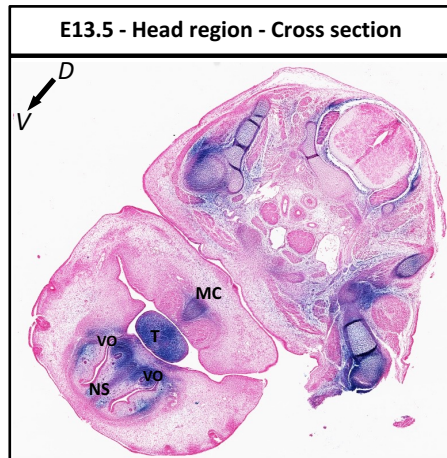
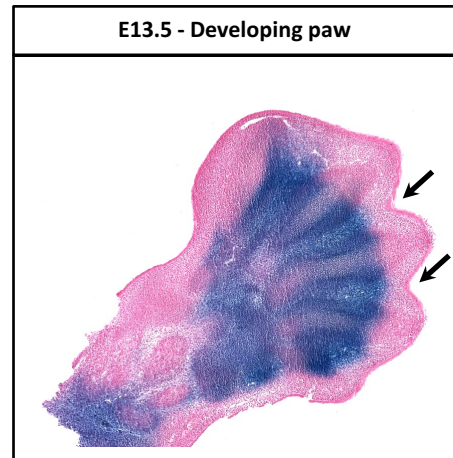


**Figure 3.****A.**

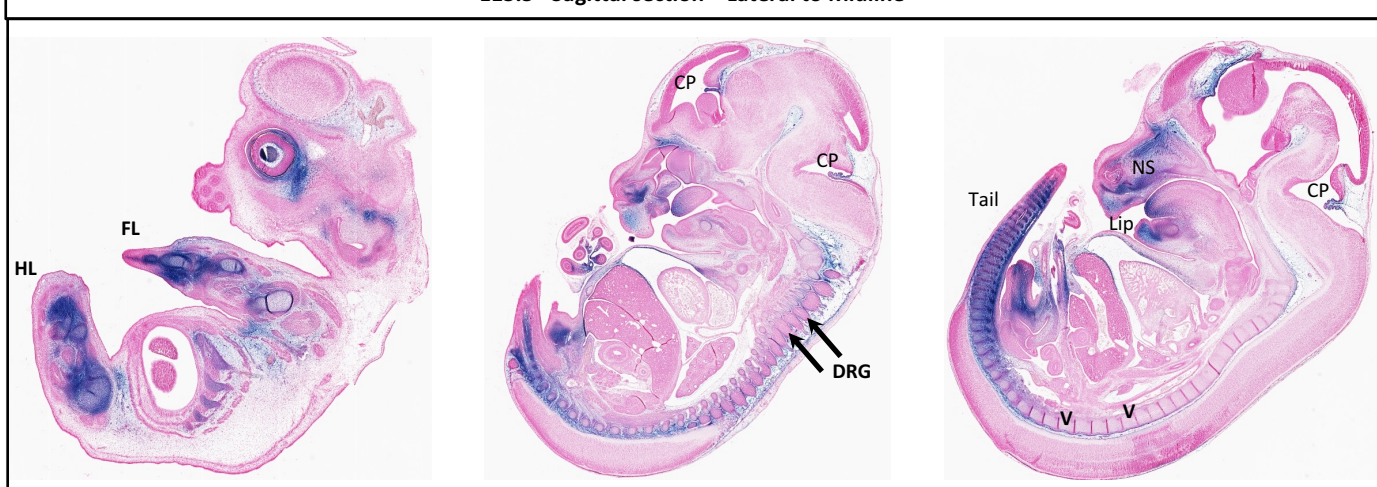
## Whole-mount

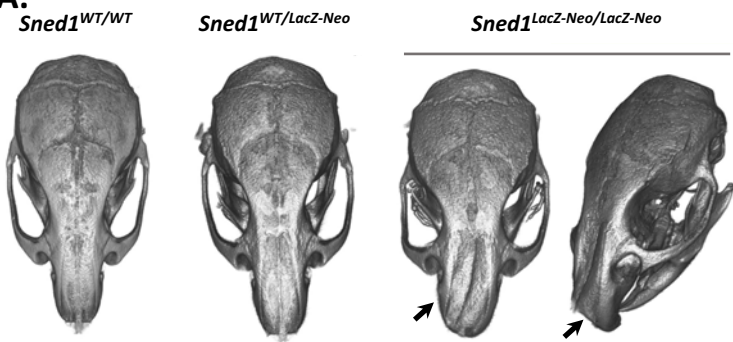
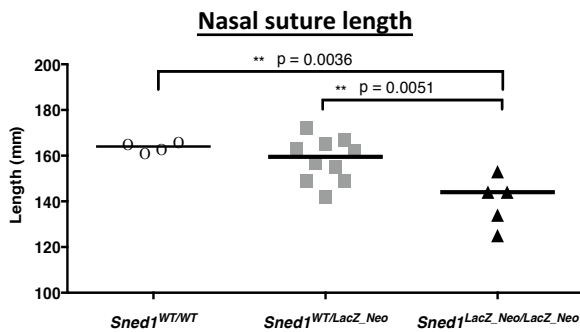
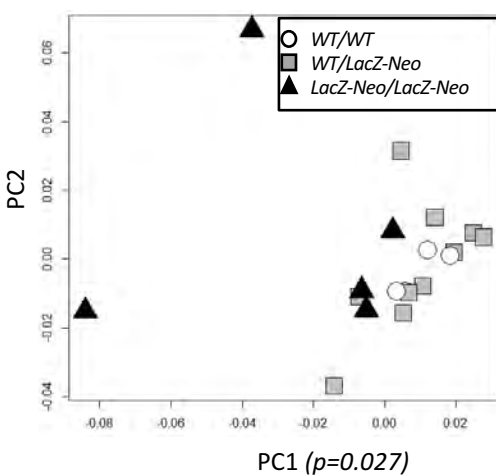
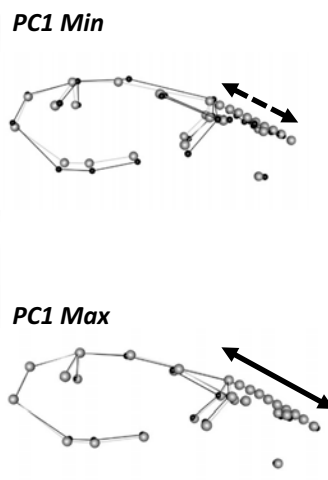
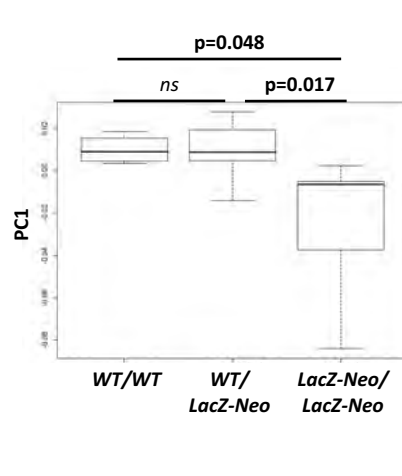
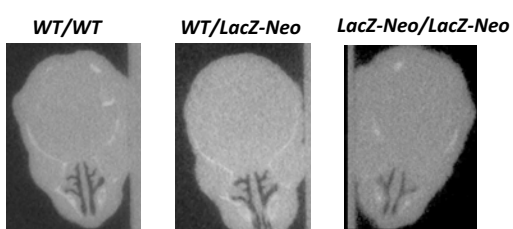
 $\beta$ -galactosidase activity assay  
*Sned1*<sup>WT/LacZ-Neo</sup> – E11.5**B.****C.****D.**

## Whole-mount

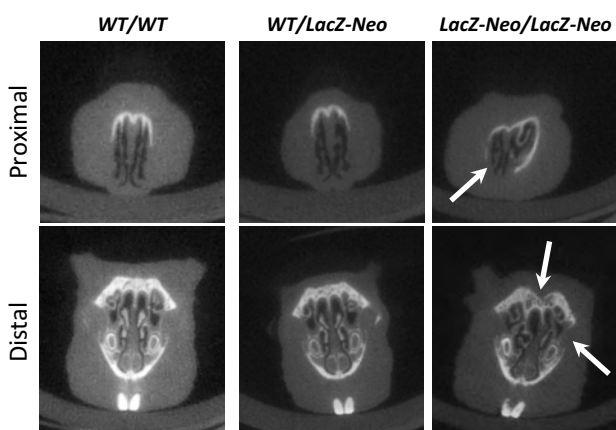
 $\beta$ -galactosidase activity assay  
*Sned1*<sup>WT/LacZ-Neo</sup> – E13.5**E.****F.****G.**

E13.5 - Sagittal section – Lateral to Midline



**Figure 4.****A.****B.****C.****D.****E.****F.**

Genotype (p0.5)	Occlusion	Symmetry
<i>Sned1</i> WT/WT	0 (0%)	4 (100%)
<i>Sned1</i> WT/NeoLacZ	3 (20%)	13 (87%)
<i>Sned1</i> LacZ-Neo/LacZ-Neo	3 (100%)	3 (100%)

**G.**

Genotype (adult)	Occlusion	Symmetry
<i>Sned1</i> WT/WT	0 (0%)	4 (100%)
<i>Sned1</i> WT/NeoLacZ	0 (0%)	9 (90%)
<i>Sned1</i> LacZ-Neo/LacZ-Neo	2 (40%)	2 (40%)